J. Electrochem. Sci. Eng. **16** (2026) 3279; https://doi.org/10.5599/jese.3279

Open Access : : ISSN 1847-9286
https://pub.iapchem.org/ojs/index.php/JESE

Original scientific paper

Electrocatalytic performance and structural characterization of NiFe phosphosulphide supported on MXene/Ni foam for hydrogen evolution reaction in alkaline and simulated alkaline seawater

Nur Quratul Ainni Muhammad Esham[1], Nurul Atiqah Izzati Md Ishak[2,✉], Suhaila Mohd Sauid[1,✉], Noor Fitrah Abu Bakar[1], Saidur Rahman[3] and Siti Kartom Kamarudin[4,5]

[1]*Faculty of Chemical Engineering, Universiti Teknologi MARA 40450, Shah Alam, Selangor, Malaysia*
[2]*Research Centre for Carbon Dioxide Capture and Utilisation (CCDCU), Faculty of Engineering and Technology, Sunway University, No. 5 Jalan Universiti, Bandar Sunway, 47500, Petaling Jaya, Selangor, Malaysia*
[3]*Research Centre for Nanomaterials and Energy Technology (RCNMET), School of Engineering and Technology, Sunway University, No. 5, Jalan Universiti, Bandar Sunway, Petaling Jaya, 47500 Selangor Darul Ehsan, Malaysia*
[4]*Fuel Cell Institute, Universiti Kebangsaan Malaysia, UKM, 43600, Bangi, Selangor, Malaysia*
[5]*Department of Chemical Engineering, Universiti Kebangsaan Malaysia, UKM, 43600, Bangi, Selangor, Malaysia*

Corresponding Authors: ✉ atiqahmi@sunway.edu.my; ✉ suhaila.sauid@uitm.edu.my

Received: March 5, 2026; Accepted: June 17, 2026; Published: June 23, 2026

Abstract

Efficient and durable electrocatalysts for the hydrogen evolution reaction in alkaline and seawater media are essential to advance green hydrogen production. In this study, a phosphorus and sulphur dual-anionic doping approach was utilized to synthesise bimetallic nickel-iron phosphosulphide (NiFePS) on $Ti_3C_2T_x$ MXene-modified nickel foam (MXene/NF) via hydrothermal growth and phosphosulphidation. Structural analysis of the NiFePS/MXene/NF using field emission scanning electron microscopy showed the formation of well-developed interconnected flower-like architectures uniformly distributed across the MXene/NF substrate. Electrochemical properties of the material were analysed using linear sweep voltammetry, electrochemical impedance spectroscopy, cyclic voltammetry and chronoamperometry. The NiFePS/MXene/NF electrocatalyst required overpotentials of 103 and 164 mV at 10 mA cm^{-2} in 1 M KOH and 1 M KOH + 0.5 M NaCl, respectively, lower than those of the undoped NiFe/MXene/NF (228 and 223 mV). NiFePS/MXene/NF also exhibited lower Tafel slopes (223 and 166 mV dec^{-1}) compared to NiFe/MXene/NF (375 and 227 mV dec^{-1}) in the respective electrolytes, along with reduced charge transfer resistance (0.64 vs. 2.45 Ω in 1 M KOH; 1.17 Ω vs. 1.29 Ω in 1 M KOH + 0.5 M NaCl). The electrocatalyst also maintained stable operation at 100 mA cm^{-2} for 24 hours in both media. These findings show that

phosphorus and sulphur co-doping offers a promising strategy to developing high-performance NiFe-based HER catalysts for both alkaline and simulated seawater electrolysis.

Keywords
Nickel-iron catalyst; MXene-modified Ni foam; dual-anionic doping; alkaline seawater electrolysis, green hydrogen production

Introduction

Green hydrogen production via water and seawater electrolysis relies on efficient electrocatalysts to govern the kinetics of the hydrogen evolution reaction (HER) and the oxygen evolution reaction (OER) [1]. Although HER is a simpler adsorption-discharge-desorption reaction than OER, its kinetics is sluggish in alkaline solutions due to the additional water dissociation step required to generate hydrogen intermediates through the Volmer-Heyrovsky or Volmer-Tafel pathways [2,3]. In seawater, additional complexity arises from the competing chlorine evolution reaction and the precipitation of insoluble salts, both of which accelerate electrocatalyst degradation and reduce productivity [4,5]. Noble-metal catalysts such as Pt are the benchmark for HER materials, but are economically impractical for large-scale electrolysis. Therefore, it is important to develop earth-abundant alternative electrocatalyst materials that are efficient, stable and cost-effective for water/seawater electrolysis.

Nickel-iron-based materials are one of the most promising non-noble HER electrocatalysts due to the tuneable redox chemistry and electronic coupling effect between Ni and Fe [6-8]. Specifically, NiFe layered double hydroxides and related oxides exhibit excellent alkaline stability but are often hindered with low intrinsic conductivity, suboptimal hydrogen adsorption energy and prone to undergo surface passivation under chloride exposure, which limit their electrocatalytic activity [9,10]. To overcome such limitations, heteroatom doping has emerged as an efficient and relatively straightforward strategy to modulate the electronic structure, enhance electrical conductivity, increase the number of electroactive sites, and improve catalyst stability [11-14]. Heteroatom doping can be implemented in various ways, depending on the dopant type and the target electrocatalytic functions. Anionic and cationic doping are the two most common strategies, and each can tailor distinct physicochemical properties of a host material. While single-element doping can enhance catalytic properties, incorporating two different dopants is more effective and provides flexibility to fine-tune catalyst's structural and electronic configuration [11,15,16]. In particular, dual-anion doping with relatively high electronegativity elements such as S, P, N, B, Se, Te, F and Cl offers greater tunability in regulating the electronic structure and surface chemistry of catalysts, thereby enhancing reaction kinetics and active-site accessibility during electrolysis [16].

For alkaline water and seawater electrolysis, various dual-anion combinations of electrocatalysts have been reported [17,18]. Among these, phosphorus and sulphur co-doping are particularly interesting and effective in modulating electronic conductivity, optimizing hydrogen adsorption energy and improving resistance to chloride-induced corrosion. P incorporation reportedly can strengthen metal-P covalency and polarize P sites, creating partially negative centres that attract protons and facilitate their discharge during the HER step. Similarly, S may form polarizable metal-S bonds that serve as basic sites for proton trapping and accelerate hydrogen adsorption [19]. These interactions thus promote faster hydrogen adsorption and desorption, leading to enhance HER kinetics. In addition, the presence of P and S dopants can generate an anion-rich surface, which could repel chloride ions in the seawater electrolyte to mitigate Cl^- induced corrosion [20]. Integrating P and S into a suitable bimetallic catalyst, such as NiFe, thus offers an effective route to maximize these benefits.

Recent studies have demonstrated the potential of NiFe-based phosphorsulphides in both alkaline and seawater media [21-25]. For instance, Song *et al*. [26] synthesized S-modified NiFe phosphate hollow microspheres that require an overpotential of 72 mV at 10 mA cm^{-2} in 1 M KOH and retained HER high activity in natural seawater. In another work, Liu *et al.* [27] developed a P, S co-doped NiFe in which the catalyst was able to deliver 500 mA cm^{-2} current at an overpotential of 289 mV in 1 M KOH and also reported minimal performance deterioration in alkaline seawater. Yu *et al*. [28] fabricated NiFePS nanotube arrays *via* sequential sulfurization-phosphorization, in which the catalyst overpotentials are only 92 mV at 10 mA cm^{-2} and 132 mV at 50 mA cm^{-2} in 1 M KOH, while exhibiting stable HER activity in saline electrolyte. Wang *et al.* [29] reported Ni_2P/NiS_2 heterointerfaces with η_{10} of 102 mV in 1 M KOH and stable hydrogen evolution during overall seawater splitting. Despite these advances, most reported NiFePS materials use multi-step phosphidation-sulfurization to achieve the dual-anion incorporation, which complicates the synthesis process and limits scalability. Further, relatively few studies have extended this dual-anion concept to seawater HER [26,27,29]. This highlights the need to simplify the material preparation methods to deliver the synergistic advantages of P and S co-doping while ensuring high HER catalytic performance and stability in both alkaline water/seawater media.

Herein, this study presents a facile phosphosulphidation route to synthesize a dual-anion-doped NiFe phosphosulfide catalyst supported on MXene-modified nickel foam (NiFePS/MXene/NF). The approach aims to simplify the multi-step phosphidation-sulfurization processes and highlight the synergistic advantages of P and S dual doping in the synthesized material. The resulting NiFePS/ /MXene/NF exhibited a well-formed hierarchical flower-like nanosheet architecture. The catalyst delivered higher HER activity than the undoped NiFe/MXene/NF electrocatalyst, with reduced charge-transfer resistance and a larger electrochemically active surface area. The conductive and hydrophilic $Ti_3C_2T_x$ MXene layer further enhances electron transport and ensures close contact between the catalyst and the NF substrate, thereby improving interfacial conductivity and stability.

Experimental

Materials and reagents

Ti_3AlC_2 MAX phase (≥ 90 %, ≤ 40 μm particle size, Sigma-Aldrich), lithium fluoride (LiF, ~300 mesh, Sigma-Aldrich), hydrochloric acid (HCl, 37 %, Fisher), ethanol (C_2H_5OH, 99.5%, Systerm), iron(III) nitrate nonahydrate ($Fe(NO_3)_3{\cdot}9H_2O$, 99 %, ThermoScientific), nickel(II) nitrate hexahydrate ($Ni(NO_3)_2{\cdot}6H_2O$, 99%, Thermoscientific), ammonium fluoride (NH_4F, 98 %, Chemiz), urea ($CO(NH_2)_2$, ≥99 %, Merck), sodium hypophosphite (NaH_2PO_2, 99 %, Sigma-Aldrich), thiourea ($C(NH_2)_2S$, 99 %, Chemiz), potassium hydroxide (KOH, >85 % purity, R&M Chemicals), sodium chloride (NaCl, >99 % purity, Chemiz), nickel foam (NF, 99.9 %, pore size ≈ 200-320 μm (80 to 120 ppi), 1 mm thickness, Fuel Cell Store).

Synthesis of $Ti_3C_2T_x$-MXene

$Ti_3C_2T_x$ MXene was synthesized from Ti_3AlC_2 MAX precursor *via* chemical etching. Firstly, 1.3 g of LiF was dissolved in 50 mL of 2.5 M HCl solution under continuous stirring at room temperature for 30 minutes. Subsequently, 1 g of Ti_3AlC_2 powder was added to the prepared etching solution and the reaction was allowed to proceed under continuous stirring at 40 °C for 24 hours to facilitate the selective etching of aluminium layers in the MAX phase precursor. After a 24-hour reaction, the resulting slurry was centrifuged, and the supernatant was discarded after the centrifugation. For the first two washing cycles, the supernatants were discarded. From subsequent washing cycles

onward, the supernatants that contained delaminated MXene nanosheets were carefully collected and stored separately. The washing step was repeated until the pH of the supernatant reached approximately 6, indicating successful removal of residual etchants and impurities. Finally, the suspension containing delaminated MXene nanosheets was collected and dried under vacuum at 60 °C for 6 hours.

Preparation of MXene/NF

The MXene dispersion was incorporated onto NF substrates using a facile immersion method. NF substrates (3× 1 cm) were initially pre-treated sequentially in 3 M HCl, 70 vol.% C_2H_5OH and deionized water for 10 minutes each to remove surface contamination and possible oxide layers. The NFs were then dried in a vacuum oven at 60 °C for 2 hours. Subsequently, the obtained dried MXene powder was dispersed in water (1 mg ml^{-1}), and the solution was ultrasonicated for 1 hour to achieve uniform dispersion. The pre-treated NFs were then immersed in the homogeneous MXene dispersion overnight to ensure sufficient adhesion and uniform coating. After the immersion, the MXene/NF were removed and dried in a convection oven at 60 °C for 2 hours.

Hydrothermal synthesis of NiFe/MXene/NF

NiFe sample precursors were synthesized on MXene/NF substrates in a hydrothermal process. In a typical synthesis, $Ni(NO_3)_2{\cdot}6H_2O$ (1 mmol), $Fe(NO_3)_3{\cdot}9H_2O$ (1 mmol), $CO(NH_2)_2$ (600 mg) and NH_4F (148.1 mg) were dissolved in 50 mL of deionized water. The solution was then stirred continuously for 2 hours at 500 rpm to ensure that all added solids were fully dissolved. Subsequently, the 4 pieces of MXene/NF obtained from the previous step were placed in a 100 mL stainless steel autoclave containing the prepared solution, sealed in and heated to 150 °C for 6 hours. After natural cooling, the synthesized NiFe/MXene/NF samples were thoroughly rinsed with deionized water several times and dried at 60 °C for 6 hours.

Phosphosulphidation of NiFe/MXene/NF

Phosphorus and sulphur co-doping was introduced into the NiFe/MXene/NF precursor sample through a phosphosulphidation annealing process. $NaPO_2H_2$ and $C(NH_2)_2S$ were used as sources of P and S, respectively. Equal masses of each powder (300 mg) were weighed and mechanically mixed using a mortar and pestle to ensure homogeneity. All 4 pieces of NiFe/MXene/NF samples from the previous step were placed downstream, each in a separate ceramic boat, while the mixture of precursors was placed upstream in the same tube furnace. Annealing was carried out at 300 °C for 2 h under a continuous argon flow with a heating rate of 5 °C min^{-1}. For comparison, a control sample of NiFe/MXene/NF was also annealed under identical conditions but without the P and S sources.

Material characterization

The surface morphology and microstructural features of the synthesized catalysts were examined using field-emission scanning electron microscopy (FESEM, Thermo Scientific Apreo 2S), equipped with energy-dispersive X-ray spectroscopy (EDX, Bruker XFlash) for elemental analysis and mapping. Crystallographic structure and phase composition were determined *via* X-ray diffraction (XRD, PANalytical X'Pert PRO). XRD measurements were conducted over a 2θ range of 5 to 90° at a scan rate of 5° min^{-1}.

Electrochemical measurements

Electrochemical performance was evaluated using a ZIVE SP2 electrochemical workstation (Zive Lab, Korea) in a conventional three-electrode configuration. The synthesized catalyst on Ni foam

(geometric exposed area = 1 cm^2) was used as the working electrode with a graphite rod and an Ag/AgCl (3 M KCl) electrode serving as the counter and reference electrodes, respectively. The reference electrode, working electrode and counter electrode were all placed in the same compartment. All measurements were performed in 1 M KOH and in 1 M KOH + 0.5 M NaCl at ambient temperature. Linear sweep voltammetry (LSV) was conducted at a scan rate of 5 mV s^{-1}. All measured potentials (E / V) were converted to the reversible hydrogen electrode (RHE) scale using Equation (1):

$$E\ (vs.\ \text{RHE}) = E\ (vs.\ \text{Ag/AgCl}) + 0.059\ \text{pH} + 0.210 \quad (1)$$

All potentials were manually corrected with partial *iR* drop using uncompensated solution resistance (R_s) values obtained from electrochemical impedance spectroscopy (EIS) measured in the respective electrolyte (1 M KOH for alkaline measurements and 1 M KOH + 0.5 M NaCl for simulated seawater measurements). EIS measurements were carried out with a 10 mV AC amplitude over a frequency range of 100 kHz to 0.01 Hz at approximately -0.97 V *vs*. RHE (equivalent to -1.3 V *vs*. Ag/AgCl in 1 M KOH and 1 M KOH + 0.5 M NaCl). Chronoamperometry (CA) was performed by fixing the potential corresponding to ~100 mA cm^{-2} and the current response was recorded for 24 h in both 1 M KOH and 1 M KOH + 0.5 M NaCl to evaluate the HER stability of the catalysts.

Results and discussion

The morphology of NiFe/MXene/NF was first examined using FESEM. At 2000× magnification (Figure 1(a)), non-uniform spherical growth was observed across the surface of the Ni foam substrate. At 5000× magnification (Figure 1(b)), this growth appeared as compact and dense flower-like structures, which could indicate a limited formation of nanosheet morphology during synthesis. The corresponding EDX spectrum and quantification in Figure 1(c) confirm the presence of Ni and Fe as the dominant transition metals in the structure, which is consistent with the intended NiFe sample phase, with S present only in trace amounts and P is absent, indicating that this sample remains undoped, consistent with the synthesis route. Oxygen is also present, suggesting the formation of hydroxide or oxide species. The detected titanium and carbon originate from the underlying MXene, partially embedded within the catalyst layer. Elemental mapping images in Figure 1(d-h) show that all the elements detected are homogeneously distributed throughout the catalyst.

The morphology of NiFePS/MXene/NF is presented in Figure 2(a). In contrast to the clustered and non-uniform spherical growth observed in the undoped NiFe/MXene/NF sample, the doped catalyst displays more abundant and well-developed flower-like spheres on the MXene/NF surface. As shown at high magnification (5000× and 10000×) in Figure 2(b) and Figure 2(c), these structures appear to assemble into flower-like structures with crumpled formations and exhibit a uniform and continuous network of nanosheets. This morphology suggests that the incorporation of P and S altered the growth of electroactive species, which promotes the formation of a more open and accessible surface that is beneficial for electrocatalytic hydrogen evolution. The EDX spectrum and corresponding elemental quantification in Figure 2(d) confirm the successful co-doping of P and S, with such elements detected in substantially higher amounts than those observed in the undoped sample.

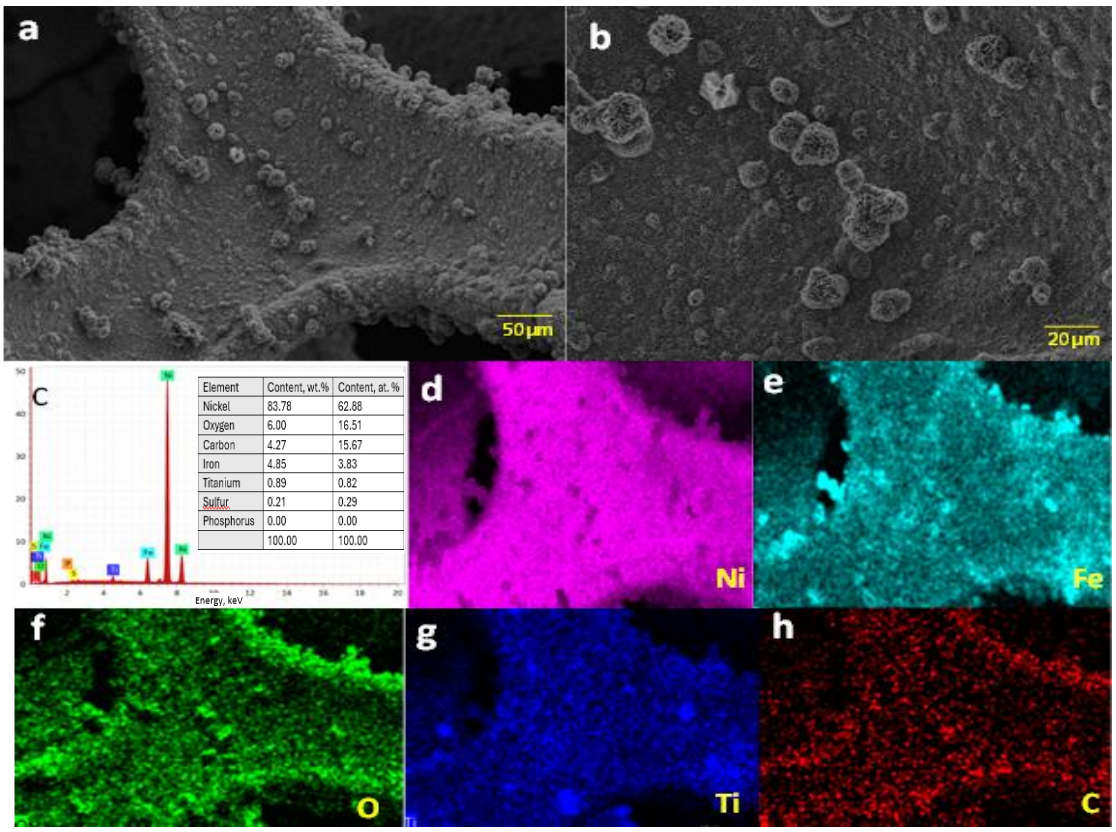

Figure 1. *(a-b) FESEM micrographs of NiFe/MXene/NF, (c) EDX spectrum and corresponding elemental quantification confirming the presence of Ni, Fe, P, S, and C elements, (d-h) elemental mapping images showing the homogeneous distribution of Ni, Fe, O, Ti, and C across the catalyst surface*

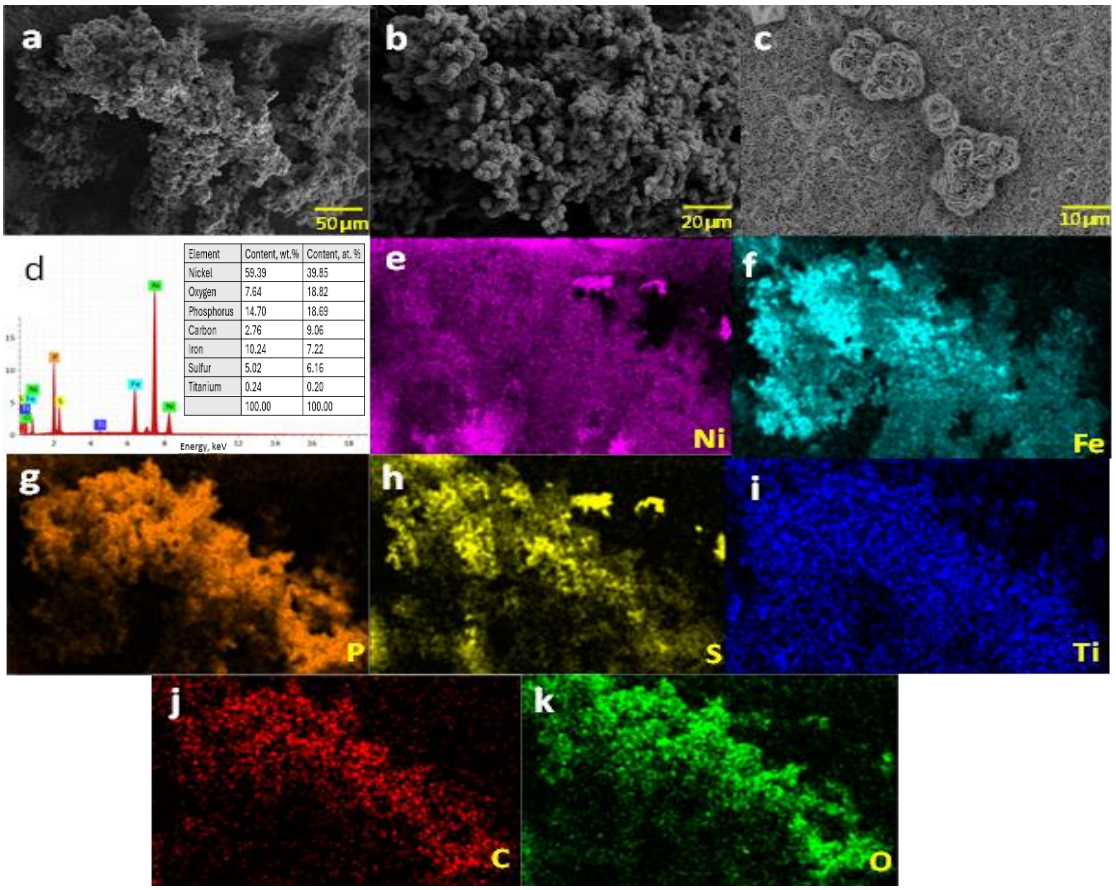

Figure 2. *(a-c) FESEM images of NiFePS/MXene/NF, (d) EDX spectrum and elemental composition confirming Ni, Fe, P, S, Ti, O and C species, (e-k) elemental mapping demonstrating uniform dispersion of all elements*

The elemental composition also includes the expected components of the NiFePS/MXene/NF catalyst sample: Ni, Fe, C, Ti, and O. Elemental mapping in Figure 2(e-k) reveals a uniform distribution of all detected elements, indicating their homogeneous dispersion across the catalyst surface. From here, it could be said that phosphosulphidation not only introduces dopants but also transforms the catalyst structure, giving rise to the interconnected, flower-like nanosheet morphology that distinguishes this sample from undoped NiFe/MXene/NF.

X-ray diffraction analysis

XRD analysis was performed to determine the crystallographic structures of NiFePS/MXene/NF and NiFe/MXene/NF. The resulting XRD patterns are shown in Figure 3. The NiFe/MXene/NF sample exhibited a significantly broader, lower-intensity diffraction pattern, suggesting low crystallinity. The absence of clear higher-order LDH peaks, such as (006), (012), or (110), is consistent with a poorly crystalline or disordered layer structure. The pattern also exhibited reflections in the 30 to 65° range consistent with the NiFeO phase (COD # 96-591-0065), as well as peaks at approximately 50 and 55° attributable to metallic Ni from the Ni foam substrate (PDF# 04-0850), suggesting a possible phase transition from LDH to mixed NiFeO/Ni phases under annealing conditions. These findings, when combined with morphological observations, imply that the undoped sample consists of a mixed phase comprising poorly crystalline LDH features and partially formed NiFeO. The lack of discernible peaks for Ni, Fe or mixed-metal phosphides and sulphides suggests an amorphous nature for the doped NiFePS/MXene/NF phase, a common characteristic of surface-doped electrocatalysts.

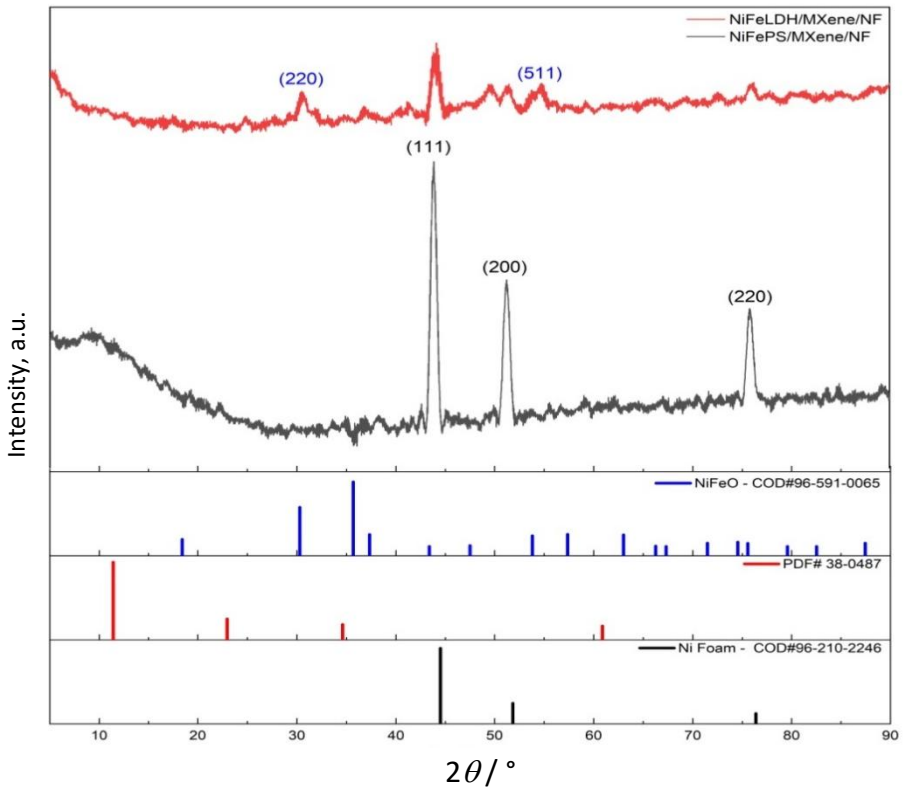

Figure 3. *XRD patterns of NiFePS/MXene/NF and NiFe/MXene/NF*

Electrochemical analysis

LSV studies were conducted in 1 M KOH and 1 M KOH + 0.5 M NaCl to evaluate and compare the HER activity of NiFePS/MXene/NF and NiFe/MXene/NF. Figure 4 shows the superior HER activity of NiFePS/MXene/NF compared to NiFe/MXene/NF in 1 M KOH. At current densities of 10, 50 and

100 mA cm^{-2} in 1 M KOH, NiFePS/MXene/NF exhibited overpotentials of 103, 256 and 321 mV, whereas NiFe/MXene/NF required 228, 408 and 531 mV, respectively. The HER performance difference between NiFePS/MXene/NF and NF widens as the current density increases. This behaviour suggests that P and S doping not only enhances the HER kinetics but also sustains high efficiency under high current operation, which is critical for practical alkaline electrolyzers. The reduced polarization slope of NiFePS/MXene/NF implies lower kinetic barriers and improved water dissociation in alkaline media. In 1 M KOH + 0.5 M NaCl, NiFePS/MXene/NF required 164, 304 and 379 mV at 10, 50 and 100 mA cm^{-2}, respectively. Although the overpotentials increase slightly in the NaCl-containing electrolyte, they remain consistently lower than those of NiFe/MXene/NF at all current densities. NiFe/MXene/NF exhibited overpotentials of 232, 327 and 395 mV under the same respective conditions. The comparatively high performance of NiFePS/MXene/NF suggests that P and S dual doping modifies the electronic structure while stabilizing the active sites and mitigating chloride-induced inhibition during electrolysis. Figure 5 further illustrates the comparison of overpotentials at the three benchmark current densities in both electrolytes.

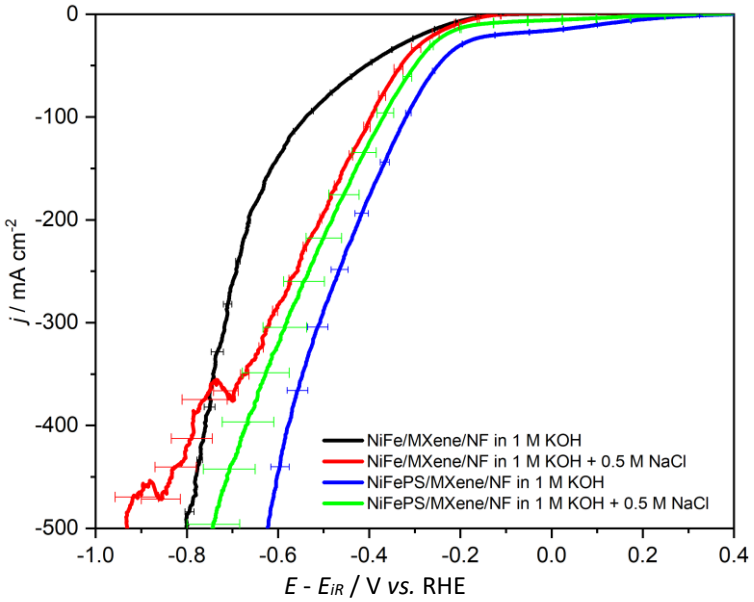

Figure 4. *LSVs of electrocatalysts acquired in 1 M KOH and 1 M KOH + 0.5 M NaCl*

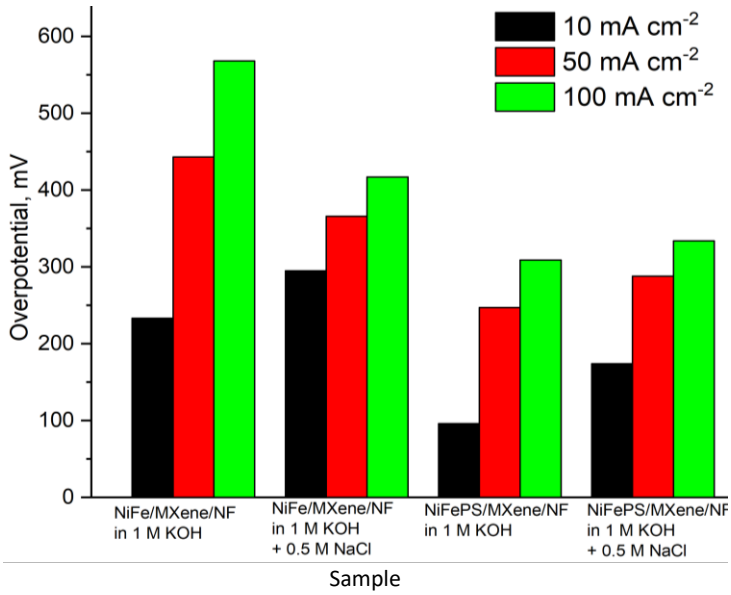

Figure 5. *Comparison of overpotentials at 10, 50 and 100 mA cm^{-2} for NiFePS/MXene/NF and NiFe/MXene/NF in 1 M KOH and 1 M KOH + 0.5 M NaCl*

The enhanced efficiency of NiFePS/MXene/NF in catalysing HER at high electrolysis rates, together with its tolerance toward chloride-rich electrolyte, is evident when compared to the non-doped sample.

HER kinetics of the synthesized catalysts were further examined using Tafel slope analysis, as shown in Figure 6. The NiFePS/MXene/NF catalyst demonstrated a significantly lower Tafel slope of 223mV dec^{-1} in 1 M KOH and 166 mV dec^{-1} in 1 M KOH + 0.5 M NaCl compared to the 375 mV dec^{-1} in 1 M KOH and 227 mV dec^{-1} in 1 M KOH + 0.5 M NaCl observed for NiFe/MXene/NF, suggesting enhanced HER kinetics due to phosphosulphidation. Tafel slopes are commonly used to infer the rate-determining step (RDS) in HER. In alkaline HER, the reaction can proceed via three elementary steps: the Volmer step (water dissociation and hydrogen adsorption, theoretical value ~118 mV dec^{-1}), the Heyrovsky step (electrochemical desorption, theoretical value ~40 mV dec^{-1}) and the Tafel step (chemical recombination, theoretical value ~30 mV dec^{-1}) [30,31]. The experimental Tafel slope for NiFePS/MXene/NF is close to the theoretical value of the Volmer step, implying that the step is the RDS. The lower slope compared to NiFe/MXene/NF suggests that dual-anionic doping creates a more favourable interface for HER, which facilitates the acceleration of water dissociation and hydrogen adsorption.

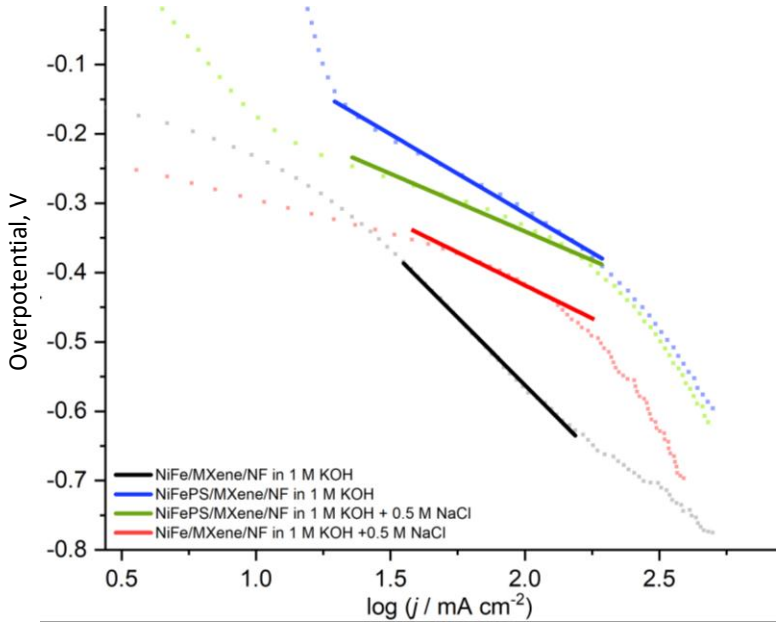

Figure 6. *Tafel slope plots of NiFePS/MXene/NF and NiFe/MXene/NF*

EIS was used to investigate the catalysts' interfacial behaviour and explain the activity differences observed in the LSV and Tafel analyses. The Nyquist plots recorded in 1 M KOH and 1 M KOH + + 0.5 M NaCl are shown in Figure 7. The data were fitted using a Randles equivalent circuit consisting of the solution resistance *(R_s)*, charge transfer resistance *(R_{ct})* and a parameter of constant phase element (*Q*), which represents non-ideal double-layer capacitance at the electrode-electrolyte interface. All fitted parameters are summarised in Table 1. In EIS analysis, a smaller semicircle in the Nyquist plot indicates a lower R_{ct}, which indicates that electrons are transferred more readily across the electrode-electrolyte interface. In 1 M KOH, NiFePS/MXene/NF exhibited an R_{ct} of 0.64 Ω, lower than 2.48 Ω for NiFe/MXene/NF, confirming faster HER charge transfer kinetics for the phosphor-sulphide-doped catalyst. In 1 M KOH + 0.5 M NaCl, the R_{ct} values were 1.17 and 1.29 Ω for NiFePS/MXene/NF and NiFe/MXene/NF, respectively. The slightly lower R_{ct} observed in the NaCl-containing electrolyte is consistent with the increased ionic strength of the solution and the

competing adsorption of chloride species at the electrode surface. Notably, NiFePS/MXene/NF maintained a significantly lower R_{ct} than NiFe/MXene/NF in both electrolytes, indicating that P and S co-doping effectively reduces the charge transfer barrier regardless of the presence of chloride ions. The EIS result justifies the lower overpotentials observed in LSV, likely due to reduced energy barriers for charge transfer, which translate into a lower applied potential required to drive the same current density. Similarly, the smaller Tafel slope obtained for NiFePS/MXene/NF confirms the sample's faster HER kinetics, following the lower interfacial resistance measured in EIS. The reduced R_{ct} is attributed to the synergistic effect of dual-doping with P and S, along with the support of MXene/NF, which has high intrinsic conductivity, typically in the range of 1 to 10 kS cm^{-1}.

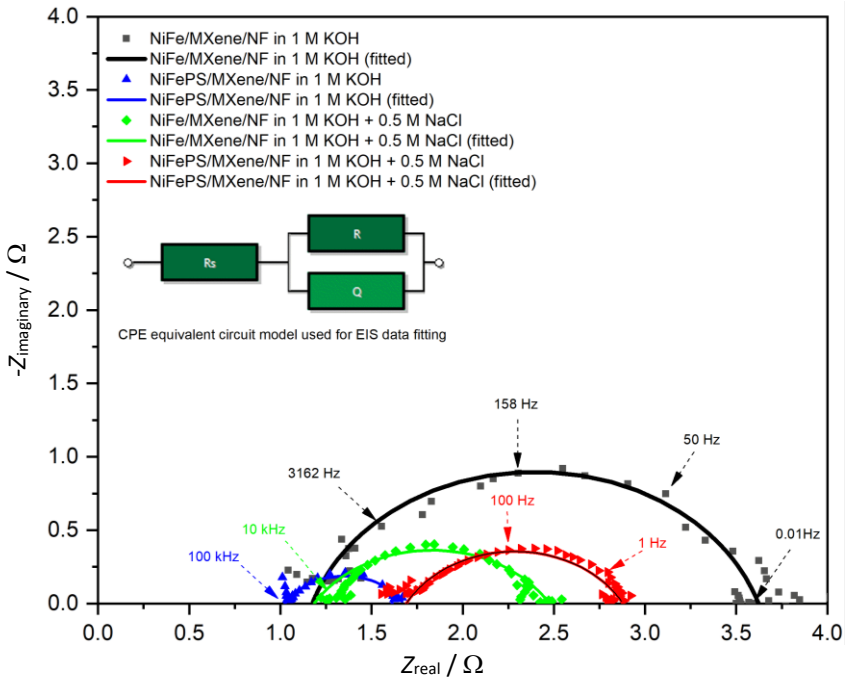

Figure 7. *Nyquist plots of NiFePS/MXene/NF and NiFe/MXene/NF recorded in 1 M KOH and 1 M KOH + 0.5 M NaCl*

Table 1. *Fitted EIS parameters obtained from the Randles-type equivalent circuit for NiFe/MXene/NF and NiFePS/MXene/NF in 1 M KOH and 1 M KOH + 0.5 M NaCl*

Sample	Electrolyte	R_s / Ω	R_{ct} / Ω	Q / S·s^n	n	χ^2	R^2
NiFe/MXene/NF	1 M KOH	1.175	2.447	0.00143	0.806	0.00649	0.990
NiFePS/MXene/NF	1 M KOH	1.026	0.639	0.276	0.671	0.00351	0.993
NiFe/MXene/NF	1 M KOH + 0.5M NaCl	1.185	1.292	0.189	0.651	0.00851	0.980
NiFePS/MXene/NF	1 M KOH + 0.5M NaCl	1.552	1.165	0.075	0.576	0.02228	0.985

Durability testing

Following the determination of enhanced HER activity and kinetics, the long-term durability of NiFePS/MXene/NF was examined using chronoamperometry. The measurements were carried out by holding the potentials corresponding to ~100 mA cm^{-2} for 24 h in both 1 M KOH and 1 M KOH + 0.5 M NaCl (Figure 8). Initially in 1 M KOH, the current density exhibited slight fluctuations before reaching gradual stabilization at around 120 mA cm^{-2} by the end of the test, which is suggested to be attributed to progressive electrode-electrolyte interfacial conditioning, including the gradual wetting and prolonged immersion of the electrode in the electrolyte solutions during the initial period of stability measurement. In 1 M KOH + 0.5 M NaCl, NiFePS/MXene/NF maintained a current

density of ~110 mA cm^{-2} with only minor fluctuations throughout the 24 h period. The absence of significant current decay highlights the catalyst stability to operate in cha loride-rich environment.

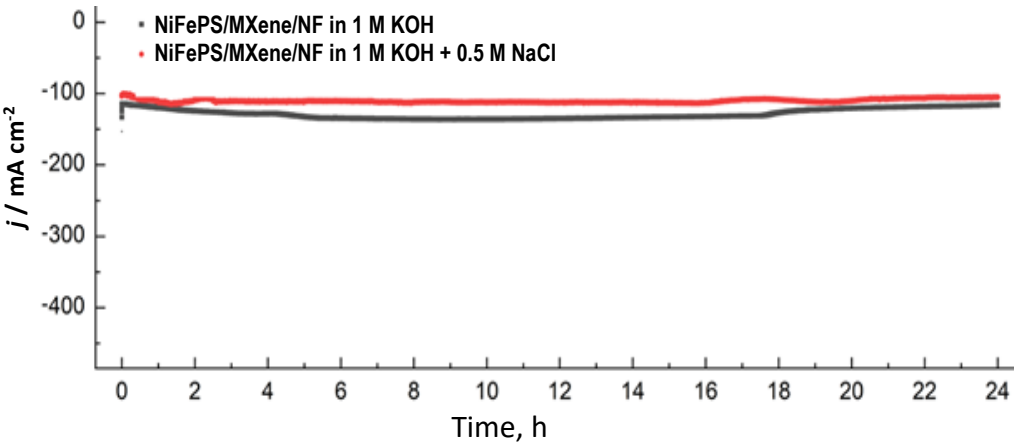

Figure 8. *Chronoamperometric stability of NiFePS/MXene/NF over 24 h*

Post-stability FESEM and EDS analyses were also conducted and shown in Figure 9. The FESEM image (Figure 9a) reveals that the characteristic flower-like nanosheet architecture is largely preserved, further indicating that the catalyst maintained its overall morphological integrity without structural collapse during prolonged HER operation in simulated alkaline solution. The EDX analysis (Figure 9b) after the stability test revealed a decrease in sulphur content from 5.02 to 3.14 wt.%, indicating partial sulphur leaching during prolonged HER operation. Nevertheless, sulphur species remained detectable after the electrochemical test, suggesting that the catalyst preserved its sulphur-containing framework and maintained reasonable compositional stability. Phosphorus shows a reduction in the surface atomic percentage relative to the pre-stability electrode, attributed to progressive surface reconstruction under cathodic polarization. This behaviour corroborates with what is commonly reported for transition metal phosphide and phosphosulphide catalysts in alkaline media, wherein surface P species undergo partial transformation into phosphate-type coordination environments at the near-surface region [2,23,32,33]. The observed decrease in surface oxygen content post-stability is consistent with the electrochemical reduction of surface oxide and hydroxide passivation layers, further corroborating the interfacial conditioning process during the initial stage of operation. Collectively, these results confirm that NiFePS/MXene/NF demonstrates satisfactory durability for HER in both alkaline and simulated seawater media.

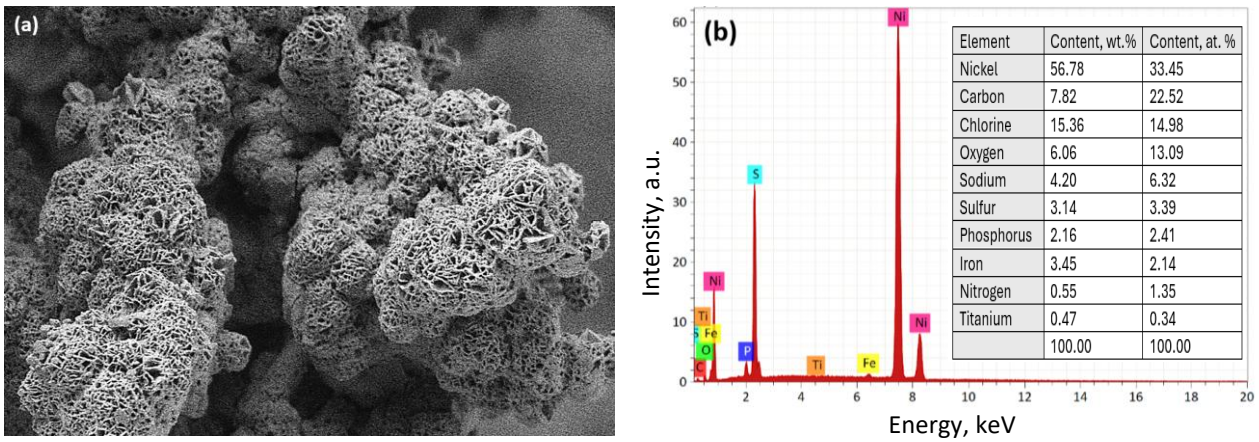

Element	Content, wt.%	Content, at. %
Nickel	56.78	33.45
Carbon	7.82	22.52
Chlorine	15.36	14.98
Oxygen	6.06	13.09
Sodium	4.20	6.32
Sulfur	3.14	3.39
Phosphorus	2.16	2.41
Iron	3.45	2.14
Nitrogen	0.55	1.35
Titanium	0.47	0.34
	100.00	100.00

Figure 9. *(a) FESEM images and (b) EDX analysis of NiFePS/MXene/NF post-HER stability test in 1 M KOH + 0.5 M NaCl*

Conclusions

In this study, a dual-anionic-doped NiFePS catalyst supported on MXene-modified NF was successfully synthesized through hydrothermal growth and a one-step phosphosulphidation process. Structural analysis and electrochemical analyses established that P and S co-doping transformed the NiFePS/MXene/NF¨morphology into a well-developed and abundant flower-like nanosheet structure. Compared with the undoped NiFe/MXene/NF, the NiFePS/MXene/NF exhibited faster HER kinetics, requiring lower overpotentials at benchmark current densities 103, 256 and 321 mV at 10, 50 and 100 mA cm^{-2} in 1 M KOH, and 164, 304 and 379 mV at the same current densities in 1 M KOH + 0.5 M NaCl. NiFePS/MXene/NF also showed lower charge-transfer resistance, 0.64 Ω in 1 M KOH and 1.17 Ω in 1 M KOH + 0.5 M NaCl, indicating desirable rapid HER activity. The alignment of these trends across complementary electrochemical analyses indicates that the overall performance enhancement of NiFePS/MXene/NF arises from the morphological transformation induced by phosphosulphidation, which generates a more open and accessible nanosheet structure, coupled with improved charge-transfer kinetics at the electrode-electrolyte interface. The catalyst also demonstrated favourable stability properties at 100 mA cm^{-2} for 24 h in both 1 M KOH and 1 M KOH + 0.5 M NaCl. These results showed that dual-anionic doping is an effective approach to enhance the HER performance of NiFe-based materials in both alkaline and simulated seawater media, and highlighted the feasibility of the presented one-step phosphosulphidation for the scalable production of an HER catalyst for green hydrogen production.

Funding: *This study was funded by the Ministry of Higher Education (MOHE) through the Fundamental Research Grant Scheme (FRGS) (FRGS/1/2023/TK08/UITM/ 02/12).*

References

[1] S. Wang, A. Lu, C.J. Zhong, Hydrogen production from water electrolysis: role of catalysts. *Nano Convergence* **8** (2021) 4. https://doi.org/10.1186/s40580-021-00254-x

[2] S. Anantharaj, S. Noda, Layered 2D PtX_2 (X = S, Se, Te) for the electrocatalytic HER in comparison with Mo/WX_2 and Pt/C: are we missing the bigger picture?. *Energy and Environmental Science* **15** (2022) 1461-1478. https://doi.org/10.1039/d1ee03516a

[3] S. Anantharaj, S. Noda, Dos and don'ts in screening water splitting electrocatalysts. *Energy Advances* (2022) 511-523. https://doi.org/10.1039/d2ya00076h

[4] H. Yuan, X. He, Y. Yang, J. Xie, B. Wu, X. Zeng, S. Zeng, Study of Fabrication and Properties of NiCoP Nanocrystalline Thin Film Electrodes for Hydrogen Evolution Electrocatalysts. *Electrocatalysis* **15** (2024) 519-528. https://doi.org/10.1007/s12678-024-00893-8

[5] Z. Zhao, J. Sun, X. Meng, Recent advances in transition metal-based electrocatalysts for seawater electrolysis. *International Journal of Energy Research* **46** (2022) 17952-17975. https://doi.org/10.1002/er.8486

[6] G. Liu, Y. Xu, T. Yang, L. Jiang, Recent advances in electrocatalysts for seawater splitting, *Nano Materials Science* **5** (2023) 101-116. https://doi.org/10.1016/j.nanoms.2020.12.003

[7] C. Feng, M. Chen, Z. Yang, Z. Xie, X. Li, S. Li, A. Abudula, G. Guan, Electrocatalytic seawater splitting for hydrogen production: Recent progress and future prospects. *Journal of Materials Science and Technology* **162** (2023) 203-226. https://doi.org/10.1016/j.jmst.2023.03.058

[8] O. Fahad Aldosari, I. Hussain, Z. Malaibari, Emerging trends of electrocatalytic technologies for renewable hydrogen energy from seawater: Recent advances, challenges, and techno-feasible assessment. *Journal of Energy Chemistry* **80** (2023) 658-688. https://doi.org/10.1016/j.jechem.2023.01.067

[9] H. Wang, H.W. Lee, Y. Deng, Z. Lu, P.C. Hsu, Y. Liu, D. Lin, Y. Cui, Bifunctional non-noble metal oxide nanoparticle electrocatalysts through lithium-induced conversion for overall water splitting. *Nature Communications* **6** (2015) 7261. https://doi.org/10.1038/ncomms8261
[10] M. Gong, D.Y. Wang, C.C. Chen, B.J. Hwang, H. Dai, A mini review on nickel-based electrocatalysts for alkaline hydrogen evolution reaction. *Nano Research* **9** (2016) 28-46. https://doi.org/10.1007/s12274-015-0965-x
[11] Z. Chen, N. Han, W. Wei, D. Chu, B.J. Ni, Dual doping: An emerging strategy to construct efficient metal catalysts for water electrolysis. *EcoEnergy* **2** (2024) 114-140. https://doi.org/10.1002/ece2.29
[12] J. Chang, G.G. Wang, Z. Yang, B. Li, Q. Wang, R. Kuliiev, N. Orlovskaya, M. Gu, Y. Du, Y. Yang, Dual-Doping and Synergism toward High-Performance Seawater Electrolysis. *Advanced Materials* **33** (2021) 2101425. https://doi.org/10.1002/adma.202101425
[13] C. Yang, K. Dong, L. Zhang, X. He, J. Chen, S. Sun, M. Yue, H. Zhang, M. Zhang, D. Zheng, Y. Luo, B. Ying, Q. Liu, A.M. Asiri, M.S. Hamdy, X. Sun, Improved Alkaline Seawater Splitting of NiS Nanosheets by Iron Doping. *Inorganic Chemistry* **62** (2023) 7976-7981. https://doi.org/10.1021/acs.inorgchem.3c00836
[14] Y. Wu, X. Du, X. Zhang, P doping transition metal sulfides as bifunctional electrocatalyst for overall seawater splitting. *International Journal of Hydrogen Energy* **103** (2025) 174-182. https://doi.org/10.1016/j.ijhydene.2025.01.181
[15] J. Zhou, Y. Bian, Z. Hao, K. Wei, J. Xiao, J. Wang, Y. Wang, H. Gou, F. Gao, Dual-doping Fe-Ni oxide for ultrahigh performance seawater oxidation by high-concentration electrolytes. *Colloids and Surfaces A* **658** (2023) 130682. https://doi.org/10.1016/j.colsurfa.2022.130682.
[16] X. Liu, J. Chi, H. Mao, L. Wang, Principles of Designing Electrocatalyst to Boost Reactivity for Seawater Splitting. *Advanced Energy Materials* **13** (2023) 2301438. https://doi.org/10.1002/aenm.202301438
[17] M. Chen, N. Kitiphatpiboon, C. Feng, A. Abudula, Y. Ma, G. Guan, Recent progress in transition-metal-oxide-based electrocatalysts for the oxygen evolution reaction in natural seawater splitting: A critical review. *EScience* **3** (2023) 100111. https://doi.org/10.1016/j.esci.2023.100111
[18] L. Zhuang, S. Li, J. Li, K. Wang, Z. Guan, C. Liang, Z. Xu, Recent Advances on Hydrogen Evolution and Oxygen Evolution Catalysts for Direct Seawater Splitting. *Coatings* **12** (2022) 659. https://doi.org/10.3390/coatings12050659
[19] S. Anantharaj, S.R. Ede, K. Sakthikumar, K. Karthick, S. Mishra, S. Kundu, Recent Trends and Perspectives in Electrochemical Water Splitting with an Emphasis on Sulfide, Selenide, and Phosphide Catalysts of Fe, Co, and Ni. *ACS Catalysis* **6** (2016) 8069-8097. https://doi.org/10.1021/acscatal.6b02479
[20] X. Wang, M. Geng, S. Sun, Q. Xiang, S. Dong, K. Dong, Y. Yao, Y. Wang, Y. Yang, Y. Luo, D. Zheng, Q. Liu, J. Hu, Q. Wu, X. Sun, B. Tang, Recent advances of bifunctional electrocatalysts and electrolyzers for overall seawater splitting. *Journal of Materials Chemistry A* **12** (2023) 634-656. https://doi.org/10.1039/d3ta06083g
[21] Y. Xue, Q. Li, A. Xie, S. Luo, Sulfur/phosphorus co-doping sequence - unlocking the key to performance enhancement of $NiFe(OH)_x$ catalyst in overall water splitting. *Fuel* **405** (2026) 136597. https://doi.org/10.1016/j.fuel.2025.136597
[22] B. Song, K. Li, Y. Yin, T. Wu, L. Dang, M. Cabán-Acevedo, J. Han, T. Gao, X. Wang, Z. Zhang, J.R. Schmidt, P. Xu, S. Jin, Tuning Mixed Nickel Iron Phosphosulfide Nanosheet Electrocatalysts for Enhanced Hydrogen and Oxygen Evolution. *ACS Catalysis* **7** (2017) 8549-8557. https://doi.org/10.1021/acscatal.7b02575

[23] D. Mukherjee, P.M. Austeria, S. Sampath, Two-Dimensional, Few-Layer Phosphochalcogenide, $FePS_3$: A New Catalyst for Electrochemical Hydrogen Evolution over Wide pH Range, *ACS Energy Letters* **1** (2016) 367-372. https://doi.org/10.1021/acsenergylett.6b00184
[24] Y. Xin, X. Kan, L.Y. Gan, Z. Zhang, Heterogeneous Bimetallic Phosphide/Sulfide Nanocomposite for Efficient Solar-Energy-Driven Overall Water Splitting. *ACS Nano* **11** (2017) 10303-10312. https://doi.org/10.1021/acsnano.7b05020
[25] C.C. Mayorga-Martinez, Z. Sofer, D. Sedmidubský, Š. Huber, A.Y.S. Eng, M. Pumera, Layered Metal Thiophosphite Materials: Magnetic, Electrochemical, and Electronic Properties. *ACS Applied Materials and Interfaces* **9** (2017) 12563-12573. https://doi.org/10.1021/acsami.6b16553
[26] S. Song, Y. Wang, X. Tian, F. Sun, X. Liu, Y. Yuan, W. Li, J. Zang, S-modified NiFe-phosphate hierarchical hollow microspheres for efficient industrial-level seawater electrolysis. *Journal of Colloid and Interface Science* **633** (2023) 668-678. https://doi.org/10.1016/j.jcis.2022.11.113
[27] S. Liu, Y. Wang, J. Gao, W. Jin, W. Xiao, L. Xin, Z. Xiao, G. Xu, C. Dai, H. Zhang, Z. Wu, L. Wang, Anionic phosphorous and sulfur regulate self-supported Ni-Fe-based electrocatalyst for water-splitting under large current density. *Fuel* **367** (2024) 131445. https://doi.org/10.1016/j.fuel.2024.131445
[28] Z. Yu, Y. Li, V. Martin-Diaconescu, L. Simonelli, J. Ruiz Esquius, I. Amorim, A. Araujo, L. Meng, J.L. Faria, L. Liu, Highly Efficient and Stable Saline Water Electrolysis Enabled by Self-Supported Nickel-Iron Phosphosulfide Nanotubes With Heterointerfaces and Under-Coordinated Metal Active Sites. *Advanced Functional Materials* **32** (2022) 2206138. https://doi.org/10.1002/adfm.202206138
[29] H.Y. Wang, J.T. Ren, L. Wang, M.L. Sun, H.M. Yang, X.W. Lv, Z.Y. Yuan, Synergistically enhanced activity and stability of bifunctional nickel phosphide/sulfide heterointerface electrodes for direct alkaline seawater electrolysis. *Journal of Energy Chemistry* **75** (2022) 66-73. https://doi.org/10.1016/j.jechem.2022.08.019
[30] S. Anantharaj, S.R. Ede, K. Karthick, S. Sam Sankar, K. Sangeetha, P.E. Karthik, S. Kundu, Precision and correctness in the evaluation of electrocatalytic water splitting: Revisiting activity parameters with a critical assessment. *Energy and Environmental Science* **11** (2018) 744-771. https://doi.org/10.1039/c7ee03457a
[31] S. Jiang, H. Suo, T. Zhang, C. Liao, Y. Wang, Q. Zhao, W. Lai, Recent Advances in Seawater Electrolysis. *Catalysts* **12** (2022) 123. https://doi.org/10.3390/catal12020123
[32] Y. Gui, Z. Liu, X. Feng, Y. Jia, Y. Zhang, Y. Zhang, H. Yang, Y. Zhang, M. Li, L. Liang, J.W. Shi, One-step electrodeposition synthesis of NiFePS on carbon cloth as self-supported electrodes for electrochemical overall water splitting. *Journal of Colloid and Interface Science* **673** (2024) 444-452. https://doi.org/10.1016/J.JCIS.2024.06.096
[33] Y. Jeung, H. Roh, K. Yong, Co-anion exchange prepared 2D structure Ni(Co,Fe)PS for efficient overall water electrolysis. *Applied Surface Science* **576** (2022) 151720. https://doi.org/10.1016/J.APSUSC.2021.151720